1   **Characteristics of Vertical Air Motion in Convective Clouds**

2

3   **Jing Yang[1], Zhien Wang[1], Andrew J. Heymsfield[2] and Jeffrey R. French[1]**

4   [1] {Department of Atmospheric Science, University of Wyoming, Laramie, WY}

5   [2] {National Center for Atmospheric Research, Boulder, CO}

6   Correspondence to: Zhien Wang (zwang@uwyo.edu)

7

8   **Abstract**

9   The vertical velocity and air mass flux in convective clouds are statistically analyzed using

10   aircraft in-situ data collected from three field campaigns: High-Plains Cumulus (HiCu)

11   conducted over the mid-latitude High Plains, COnvective Precipitation Experiment (COPE)

12   conducted in a mid-latitude coastal area, and Ice in Clouds Experiment-Tropical (ICE-T),

13   conducted over a tropical ocean. This study yields the following results. (1) Small-scale updrafts

14   and downdrafts (< 500 m in diameter) are frequently observed in the three field campaigns, and

15   they make important contributions to the total air mass flux. (2) The probability density functions

16   (PDFs) of the vertical velocity are exponentially distributed. For updrafts, the PDFs of the

17   vertical velocity are broader in ICE-T and COPE than in HiCu; for downdrafts, the PDFs of the

18   vertical velocity are broader in HiCu and COPE than in ICE-T. (3) Vertical velocity profiles

Atmospheric
Chemistry
and Physics
Discussions

Open Access

EGU

19   show that updrafts are stronger in ICE-T and COPE than in HiCu, and downdrafts are stronger in

20   HiCu and COPE than in ICE-T. (4) The PDFs of the air mass flux are exponentially distributed

21   as well. The maximum air mass flux in updrafts is of the order 10^4 kg m^{-1} s^{-1}. The air mass flux

22   in the downdrafts is typically a few times smaller in magnitude than that in the updrafts.

23

24   **1.   Introduction**

25   Convective clouds are an important component of the global energy balance and water cycle

26   because they dynamically couple the planetary boundary layer to the free troposphere through

27   vertical heat, moisture and mass transport (Arakawa, 2004; Heymsfield et al., 2010; Wang and

28   Geerts, 2013). The vertical velocity determines the vertical transport of cloud condensate, the

29   cloud top height and the detrainment into anvils, which further impact the radiative balance (Del

30   Genio et al., 2005). Vertical velocity also has significant impact on the aerosol activation, droplet

31   condensation and ice nucleation in convective clouds, which control the cloud life cycle and

32   precipitation efficiency.

33   In order to reasonably simulate convective clouds, the vertical air velocity must be parameterized

34   reliably in numerical weather prediction models (NWPMs) and global circulation models (GCMs)

35   (Donner et al., 2001; Tonttila et al., 2011; Wang and Zhang, 2014). However, the complexity of

36   the vertical velocity structure in convective clouds makes the parameterization non-

37   straightforward (Wang and Zhang, 2014). Observations show that in most of the convective

38   clouds the vertical velocity is highly variable, and consequently the detailed structure of

39   convection cannot be resolved in many models (Kollias et al., 2001; Tonttila et al., 2011).

Atmospheric
Chemistry
and Physics
Discussions

40   Additionally, using the same parameterization of vertical velocity for different grid resolutions

41   may result in different cloud and precipitation properties (Khairoutdinov et al., 2009).

42   Furthermore, poorly parameterized vertical velocity may result in large uncertainties in the

43   microphysics; for instance, the cloud droplet concentration may be underestimated due to

44   unresolved vertical velocity (Ivanova and Leighton, 2008). Vertical velocity simulated by

45   models with horizontal resolutions down to a few hundred meters may be more realistic (e.g. Wu

46   et al., 2009), but more observations are needed to evaluate this suggestion.

47   Aircraft in-situ measurement has been the most reliable tool enabling us to understand the

48   vertical velocity in convective clouds and to develop the parameterizations for models. Early

49   studies (e.g. Byers and Braham, 1949; Schmeter, 1969) observed strong updrafts and downdrafts

50   in convective clouds; however, their results have a large uncertainty, because the aircrafts were

51   not equipped with inertial navigation systems (LeMone and Zipser, 1980). In 1974, the Global

52   Atmospheric Research Program (GARP) Atlantic Tropical Experiment (GATE) was conducted

53   off the west coast of Africa, focusing on tropical maritime convections (Houze, 1981). A series

54   of findings based on the aircraft data collected from the project was reported. For example, the

55   accumulated probability density functions (PDFs) of vertical velocity and diameter of the

56   convective cores are lognormal distributed. The updrafts and downdrafts in GATE (tropical

57   maritime clouds) were only one half to one third as strong as those observed in the Thunderstorm

58   Project (continental clouds) (LeMone and Zipser, 1980; Houze, 1981). These findings stimulated

59   later statistical studies of the vertical velocity in convective clouds. Jorgensen et al. (1985) found

60   that the accumulated PDFs of vertical velocity in intense hurricanes were also lognormal

61   distributed and the strength was similar to that in GATE, but the diameter of the convective

62   region was larger. Studies of the convective clouds over Taiwan (Jorgensen and LeMone, 1989)

Atmospheric
Chemistry
and Physics

Discussions

63   and Australia (Lucas et al., 1994) showed a magnitude of vertical velocity similar to that in

64   GATE. Although the results from the Thunderstorm Project are suspect, the significantly

65   stronger drafts reveal the possible difference between continental and tropical maritime

66   convective clouds. Lucas et al. (1994) suggested that the water loading and entrainment strongly

67   reduce the strength of updrafts in maritime convections. However, this underestimation of the

68   updraft intensity may be also due to the sampling issues, e.g. penetrations were made outside the

69   strongest cores (Heymsfield et al., 2010).

70   There are a few more recent aircraft measurements (e.g. Igau et al, 1999; Anderson et al., 2005),

71   but the data are still inadequate to fully characterize the vertical velocity in convective clouds. In

72   most of these earlier papers, the defined draft or draft core required a diameter no smaller than

73   500 m; this threshold excluded many narrow drafts with strong vertical velocity and air mass

74   flux. In addition, the earlier studies used 1-Hz resolution data, which can resolve only the vertical

75   velocity structures larger than a few hundred meters, but the narrow drafts may be important to

76   the total air mass flux exchange and cloud evolution. Furthermore, previous aircraft observations

77   for continental convective clouds were based only on the Thunderstorm Project; thus, new data

78   are needed to study the difference between continental and maritime convections.

79   Remote sensing by means of, for example, wind profilers and radars is another technique which

80   has often been used in recent years for studying the vertical velocity in convective clouds (e.g.

81   Kollias et al., 2001; Hogan et al., 2009; Schumacher et al., 2015). Using profiler data, May and

82   Rajopadhyaya (1999) analyzed the vertical velocity in deep convections near Darwin, Australia.

83   They observed that the updraft intensified with height and that the maximum vertical velocity

84   was greater than 15 m s^{-1}. Heymsfield et al. (2010) studied the vertical velocity in deep

85   convection using an airborne nadir-viewing radar. Strong updrafts were observed over both

86   continental and ocean areas, with the peak vertical velocity exceeding 15 m s^{-1} in most of the

87   cases and exceeding 30 m s^{-1} in a few cases. Zipser et al. (2006) used satellite measurements to

88   find the most intense thunderstorms around the world; they applied a threshold updraft velocity

89   greater than 25 m s^{-1} to identify intense convection. Remote sensing has the advantage of being

90   able to measure the vertically velocity at different heights simultaneously (Tonttila et al., 2011).

91   However, remote sensing measurements are not as accurate as aircraft measurements, because

92   many assumptions are needed to account for the contribution of particle fall speed in the

93   observed Doppler velocity in order to ultimately estimate air velocity. In addition, ground-based

94   radars can rarely provide good measurements over oceans, and airborne cloud radars often suffer

95   from the attenuation and non-Rayleigh scattering in convective clouds. Therefore, in-situ

96   measurements are still necessary in order to characterize the dynamics in convective clouds and

97   to develop parameterizations for models.

98   The present study provides aircraft data analysis of the updrafts and downdrafts in mid-latitude

99   continental, mid-latitude coastal and tropical maritime convective clouds using the fast-response

100   in-situ measurements collected from three field campaigns: the High-Plains Cumulus (HiCu), the

101   COnvective Precipitation Experiment (COPE) and the Ice in Clouds Experiment-Tropical (ICE-

102   T). All the clouds formed in isolation, but some of them merged as they evolved. Statistics of the

103   vertical velocity and air mass flux are provided. The Wyoming Cloud Radar (WCR), onboard the

104   aircraft, is used to identify the cloud top height, and high frequency (25-Hz) in-situ

105   measurements of vertical velocity are used to generate the statistics. Section 2 describes the

106   datasets and wind measuring systems. Section 3 presents the analysis method. Section 4 shows

107   the results, and conclusions are given in Section 5.

Atmospheric
Chemistry
and Physics
Discussions

108

2.   Dataset and instruments

2.1   Dataset

111   The data used in the present study were collected from three field campaigns: HiCu, COPE and

112   ICE-T. Vigorous convective clouds were penetrated during the three field campaigns, including

113   mid-latitude continental, mid-latitude coastal, and tropical maritime convective clouds. These

114   penetrations provide good quality measurements for studying the microphysics and dynamics in

115   the convective clouds, as well as the interactions between the clouds and the ambient air. The

116   locations of the three field campaigns are shown in Fig. 1. Information regarding the penetrations

117   used in this study is summarized in Table 1.

118   The HiCu project was conducted mainly in Arizona and Wyoming (Fig. 1) from 18 July to 05

119   August 2002 and from 07 July to 31 August 2003 to investigate the microphysics and dynamics

120   in convective clouds over mid-latitude High Plains. The University of Wyoming King Air

121   (UWKA) was operated as the platform. In 2002 and 2003, 10 and 30 research flights were made,

122   respectively. In this study, the 2002 HiCu and 2003 HiCu are analyzed together because they

123   were both conducted over the High Plains and the sample size of 2002 HiCu is relatively small.

124   Fast-response in-situ instruments and the Wyoming Cloud Radar (WCR, Wang et al., 2012) were

125   operated during the field campaign to measure the ambient environment, cloud dynamics and

126   microphysics as well as two-dimensional (2D) cloud structure. As shown in Table 1, penetrations

127   in HiCu were made between 2 km and 10 km MSL. The sample size is relatively good below 8

128   km and relatively small above 8 km. The aircraft flew about 2000 km in clouds. In-situ

Atmospheric
Chemistry
and Physics
Discussions

129   measurements and WCR worked well in these flights; however, the upward-pointing radar was

130   operated in less than half of the research flights, and thus only a sub-set of the cloud tops can be

131   estimated. Fig. 2a(1–3) shows an example of the clouds sampled in HiCu, including WCR

132   reflectivity, Doppler velocity and 25-Hz in-situ measurement of the vertical velocity. In HiCu,

133   both developing and mature convective clouds were penetrated; some penetrations were near

134   cloud top, while most of them were more than 1 km below cloud top. From the Doppler velocity

135   and the in-situ vertical velocity, we can see that, in both the developing and mature cloud, strong

136   updrafts and downdrafts were observed, and multiple updrafts and downdrafts existed in the

137   same cloud.

138   The COPE project was conducted from 03 July to 21 August, 2013 in Southwest England (Fig.

139   1). The UWKA was used to study the microphysics and entrainment in mid-latitude coastal

140   convective clouds (Leon et al., 2015). Seventeen research flights were conducted; penetrations

141   focused on regions near cloud top, which is verified based on the radar reflectivity from the

142   onboard WCR. Since COPE was conducted in a coastal area, the convection initiation

143   mechanism is different from that over a purely continental or ocean area. In addition, although

144   the ambient air mainly came from the ocean, continental aerosols might be brought into clouds,

145   since many of the convective clouds formed within the boundary layer, which further affects the

146   microphysics and dynamics in the clouds. The measurements made in COPE include temperature,

147   vertical velocity, liquid water content, and particle concentration and size distributions. The

148   WCR provided excellent measurements of reflectivity and Doppler velocity. The downward

149   Wyoming Cloud Lidar (WCL) was operated to investigate the liquid (or ice) dominated clouds.

150   Between 0 km and 6 km, about 800 penetrations were made. Flight distance in cloud totaled

151   about 1000 km. The sample sizes are relatively good between 2 km and 6 km, but relatively

Atmospheric
Chemistry
and Physics
Discussions

152   small between 0 km and 2 km. Examples of the penetrations are given in Fig. 2b(1–3). COPE has

153   fewer penetrations than HiCu, and most of the penetrations are near the cloud top. Fig. 2b(2)

154   reveals relatively simple structures of the updrafts and downdrafts in COPE compared to HiCu,

155   but as shown by the 25-Hz in-situ vertical velocity measurement in Fig. 2b(3), there are still

156   many complicated fine structures in the vertical velocity distribution.

157   The ICE-T project was conducted from July 1 to July 30, 2011 near St. Croix, U.S. Virgin

158   Islands (Fig. 1), with state-of-the-art airborne in situ and remote sensing instrumentations, with

159   the aim of studying the role of ice generation in tropical maritime convective clouds. The

160   NSF/NCAR C-130 aircraft was used during ICE-T to penetrate convective clouds over the

161   Caribbean Sea. Thirteen C-130 research flights were conducted during the field campaign, with

162   vigorous convective clouds penetrated. In-situ measurements from ICE-T include the liquid and

163   total condensed water contents, temperatures, vertical velocities, and cloud and precipitating

164   particle concentrations and size distributions. The WCR was operated on seven research flights

165   to measure the 2D reflectivity and Doppler velocity fields. The aircraft flew more than 1500 km

166   in clouds, and more than 650 cloud penetrations were made between 0 km and 8 km. The sample

167   sizes are good except between 2 km and 4 km (Table 1). Examples of the penetrations are shown

168   in Fig. 2c(1–3). During ICE-T, clouds in different stages were penetrated, including developing,

169   mature and dissipating, some near cloud top and some considerably below cloud top. Strong

170   updrafts were observed in the developing and mature clouds, but the downdrafts in ICE-T are

171   typically weaker than those in HiCu and COPE. The vertical velocity structures are complicated,

172   as confirmed by both the Doppler velocity and the 25-Hz in-situ measurement. Weak updrafts

173   and downdrafts were also observed in the dissipating clouds.

Atmospheric
Chemistry
and Physics
Discussions

174

2.2   Wind measuring system

176   On both C-130 and UWKA, A Radome Five-Hole Gust Probe is installed for three-dimensional

177   (3D) wind measurement. A Radome Five-Hole Gust Probe is an aircraft radome probe with five

178   pressure ports installed in a "cross" pattern. Relative wind components (e.g. true air speed and

179   flow angles) are sensed by a combination of differential pressure sensors attached to the five

180   holes (Wendisch and Brenguier, 2013). Detailed calculation of relative wind components is

181   described in Kroonenberg et al. (2008) and Wendisch and Brenguier (2013). The time response

182   and the accuracy of the pressure sensors is about 25 Hz and 0.1 mb. The 3D wind vectors can be

183   derived by taking out the aircraft motions from the relative wind measurement. On both C-130

184   and UWKA, the aircraft motion is monitored by a Honeywell Laseref SM Inertial Reference

185   System (IRS), with an accuracy of 0.15 m s^{-1} for vertical motion. Global Positioning System

186   (GPS) was applied to remove the drift errors in the IRS position in all the three field campaigns

187   (Khelif et al., 1998). The final vertical wind velocity product has an accuracy of about ±0.2 m s^{-1},

188   and a time response of 25 Hz. This uncertainty (±0.2 m s^{-1}) is a mean bias. For each output, the

189   uncertainty is related to the true air speed, aircraft pitch angle, roll angle and ambient conditions.

190   Therefore, the random error varies and could be larger than the mean bias. More information

191   about the wind measurement on C-130 and UWKA can be found on the C-130 Investigator

192   Handbook (available on https://www.eol.ucar.edu/content/c-130-investigator-handbook) and

193   UWKA Investigator Handbook (available on

194   http://www.atmos.uwyo.edu/uwka/users/KA_InstList.pdf)

195

Atmospheric
Chemistry
and Physics
Discussions

196   3.   Analysis method

197   3.1   Identifying cloud using in-situ measurements

198   The Particle Measuring Systems (PMS) Two-Dimensional Cloud (2D-C) Probe and the Forward

199   Scattering Spectrometer Probe (FSSP) are often used to characterize cloud microphysics (e.g.

200   Anderson et al., 2004), although different thresholds of 2D-C and FSSP concentrations are

201   usually used to identify the edge of a cloud. In this paper, we also use FSSP and 2D-C probes to

202   find the cloud edges. In order to find a reasonable threshold for identifying cloudy air, we first

203   use the WCR reflectivity to identify the clouds and the cloud-free atmosphere; for those regions

204   we then plot the particle concentrations measured by FSSP and 2D-C in order to determine the

205   reasonable thresholds, and we apply the thresholds of particle concentrations to all the research

206   flights without WCR.

207   To identify clouds using WCR, the six effective range gates nearest to the flight level (three

208   above and three below) are chosen in each beam. Any beam in which the minimum reflectivity at

209   the six gates exceeds the noise level[1] is identified as in cloud.

210   Fig. 3 shows the occurrence distribution as a function of the particle concentrations measured by

211   FSSP versus the concentrations of the particles ≥ 50 μm in diameter measured by 2D-C in the

212   clouds identified by WCR reflectivity. From the figure, we can see that the FSSP concentration

213   ranges from 0.01 cm^{-3} to 1000 cm^{-3}, and the 2D-C concentration ranges from 0.1 L^{-1} to 10000 L^{-1}.

214   Generally, shallow clouds have relatively higher concentrations of small particles and lower

---

[1] Based on the reflectivity measured in cloud-free air, the noise level of WCR reflectivity is -32 dBZ at a range of
500 m and -28 dBZ at a range of 1000 m. In this study, we choose -30 dBZ as the threshold to identify cloud. This
threshold is examined for all three field campaigns.

Atmospheric
Chemistry
and Physics
Discussions

215   concentration of particles larger than 50 μm. In deeper convective clouds, high concentrations

216   can be seen for both small and large particles. The FSSP concentrations in cloud-free air are

217   found to be 2 cm^{-3} at most, and the FSSP concentrations measured below the lifting condensation

218   level (LCL), where precipitating particles dominated, are lower than 2 cm^{-3}, as well. Therefore, 2

219   cm^{-3} is selected as the concentration threshold to identify clouds based on the FSSP

220   measurements, as shown by the dashed line in Fig. 3. However, in some clouds (e.g. pure ice

221   clouds), the FSSP concentration could be lower than 2 cm^{-3}, and 2D-C concentrations are needed

222   to identify these cold clouds. We chose a 1 L^{-1} 2D-C concentration for particles ≥ 50 μm as the

223   second threshold to identify cloud, as shown by the dotted line in Fig. 3. In order to avoid

224   precipitating regions (below the LCL calculated from soundings), the second threshold is only

225   applied to penetrations at temperatures colder than 0 ℃; thus the cloud is defined as FSSP

226   concentration ≥ 2 cm^{-3} or 2D-C concentration ≥ 1 L^{-1}. At temperatures warmer than 0 ℃, the

227   FSSP concentrations in most of the convective clouds are higher than 2 cm^{-3}, so only the first

228   threshold is used.

229   Once a cloud is identified, the penetration details can be calculated, including the flight length,

230   the flight height, the cloud top height if WCR is available, and the penetration diameter. The

231   penetration diameter is calculated as the distance between the entrance and exit of a penetration.

232   In order to reject whirl penetrations and penetrations with significant turns, we require that the

233   diameter of a penetration be at least 90% of the flight length. The penetration diameter can

234   generally reveal the scale of a cloud, but since the aircraft may not penetrate exactly through the

235   center of a cloud, the actual cloud diameter may be larger than the penetration diameter. Based

236   on WCR reflectivity images, there are no isolated convective clouds larger than 20 km in

237   diameter. There are a few penetrations longer than 20 km, but these clouds are more like

238   mesoscale convective systems (MCS), and so they are excluded from this study.

239

240   **3.2   Defining updraft and downdraft**

241   In previous studies of the vertical velocity based on in-situ measurements, the updraft and

242   downdraft are often defined as an ascending or subsiding air parcel with the vertical velocity

243   continuously ≥ 0 m s^{-1} in magnitude and ≥ 500 m in diameter (e.g. LeMone and Zipser, 1980;

244   Jorgensen and LeMone, 1989; Lucas et al., 1994; Igau et al., 1999). In this study, we use a

245   vertical velocity threshold of 0.2 m s^{-1}, that is, the draft has a vertical velocity continuously ≥ 0.2

246   m s^{-1} in magnitude, because ± 0.2 m s^{-1} is the accuracy of the instrument. Any very narrow and

247   weak portion (diameter < 10 m and maximum vertical velocity < 0.2 m s^{-1} in magnitude)

248   between two relatively strong portions is ignored, and the two strong portions are considered as

249   one draft.

250   The diameter threshold (500 m) is not used in this paper, because drafts narrower than 500 m

251   frequently occur and they make important contributions to the total air mass flux in the

252   atmosphere and therefore they are necessarily to be considered in model simulations. Fig. 4

253   shows the PDFs of the diameters of all the updrafts and downdrafts sampled in HiCu, COPE and

254   ICE-T. In all the panels, the diameters are exponentially distributed, the PDFs can be fitted using

255    $$f = \alpha \cdot |x|^{\beta} \cdot \exp(\gamma|x|) \qquad (1)$$

Atmospheric
Chemistry
and Physics
Discussions

Open Access

256   where f is the frequency and x is the diameter. The coefficients α, β and γ for each PDF is shown

257   in each panel. This function will also be used to fit the PDFs of vertical velocity and air mass

258   flux in the following analyses. Generally, as seen in Fig 4, the PDFs broaden with height

259   increases for the three field campaigns; this is consistent with previous findings (LeMone and

260   Zipser, 1980). The diameters of the updrafts are smaller in COPE compared to those sampled in

261   HiCu and ICE-T, possibly because most of the penetrations are near cloud top. The diameters of

262   the downdrafts are relatively small in HiCu. ICE-T has the most drafts with diameters exceeding

263   100 m, and the average diameters in ICE-T for both updrafts and downdrafts are the largest. As

264   shown in Fig. 4, many narrow drafts are observed. More than 85%, 90% and 74% of the updrafts

265   are narrower than 500 m (dotted lines) in HiCu, COPE and ICE-T, respectively, and more than

266   90% of the downdrafts in all three field campaigns are narrower than 500 m. A threshold of 500

267   m in diameter would exclude many small-scale drafts, therefore, in this study all the drafts

268   broader than 50 m (dashed lines) are included. The drafts narrower than 50 m are excluded

269   because most of them are turbulences and they can hardly be resolved in models.

270   Fig. 5a shows the occurrence distributions as a function of the mean vertical velocity versus the

271   diameter of the drafts with the vertical velocity continuously ≥ 0.2 m s^{-1} in magnitude. From the

272   figure, it is noted that many drafts narrower than 500 m have quite strong vertical velocities. The

273   maximum mean vertical velocity of these narrow drafts can reach 8 m s^{-1}, and the minimum

274   mean vertical velocity in the downdrafts is -6 m s^{-1}. With such strong mean vertical velocity,

275   narrow drafts could contribute noticeably to the total air mass flux. Fig. 5b presents the

276   occurrence distributions as a function of the air mass flux versus the diameter of the drafts. The

277   air mass flux is calculated as $\bar{\rho}\bar{w}D$ (LeMone and Zipser, 1980), where $\bar{\rho}$ is the mean air density

278   at the measurement temperature, $\bar{w}$ is the mean vertical velocity and D is the diameter of each

Atmospheric
Chemistry
and Physics
Discussions

279   draft. Fig. 5b shows that the air mass flux in many drafts narrower than 500 m is actually larger

280   than that in some of the broader drafts. The maximum value for these narrow updrafts reaches

281   4000 kg m^{-1} s^{-1}, and the minimum value for the downdrafts reaches –3000 kg m^{-1} s^{-1}. The

282   normalized accumulated flux (red curves) reveals that the drafts narrower than 500 m (dotted

283   horizontal lines) make very significant contributions to the total air mass flux. Calculations

284   indicate that the updrafts narrower than 500 m contribute 20%–35% of the total upward flux, and

285   that the downdrafts narrower than 500 m contribute 50%–65% of the total downward air mass

286   flux. Drafts narrower than 50 m (dashed horizontal lines), which are excluded in this paper,

287   contributes less than 5% of the total air mass flux.

288   In this study, we delineate three different groups of updraft and downdraft using three thresholds

289   of air mass flux: 10 kg m^{-1} s^{-1}, 100 kg m^{-1} s^{-1} and 500 kg m^{-1} s^{-1} in magnitude., The air mass flux

290   is used here to delineate the draft intensity because (1) air mass flux contains the information of

291   both vertical velocity and draft size; (2) air mass flux can reveal the vertical mass transport

292   through convections; and (3) air mass flux is an important component in cumulus and convection

293   parameterizations (e.g. Tiedtke, 1989; Bechtold et al., 2001). The first designated group, the

294   "weak draft," with air mass flux 10–100 kg m^{-1} s^{-1} in magnitude, contributes 10% of the total

295   upward air mass flux and 10% of the total downward air mass flux. The "moderate draft," with

296   air mass flux 100–500 kg m^{-1} s^{-1} in magnitude, contributes 25% of the total upward air mass flux

297   and 40% of the total downward air mass flux. The "strong draft," where the air mass flux ≥ 500

298   kg m^{-1} s^{-1} in magnitude contributes 60% of the total upward air mass flux and 20% of the total

299   downward air mass flux. Drafts weaker than 10 kg m^{-1} s^{-1} are not analyzed because they are too

300   weak and most of them are very narrow and can hardly be resolved in models (Fig. 5b). The

301   numbers of weak, moderate and strong updrafts and downdrafts sampled at 0–2 km, 2–4 km, 4–6

302   km, 6–8 km and 8–10 km MSL are shown in Table 2. Generally, weak and moderate drafts are

303   more often observed than strong drafts. At most of the height ranges, more updrafts are observed

304   than downdrafts.

305   Some researchers have defined a "draft core" by selecting the strongest portion in a draft. For

306   example, LeMone and Zipser (1980) define an updraft core as an ascending air motion with

307   vertical velocity continuously ≥ 1 m s^{-1} and diameter ≥ 500 m. This definition of a "draft core" is

308   followed in a few more recent studies (e.g. Jorgensen and LeMone, 1989; Lucas et al., 1994;

309   Igau et al., 1999). We too analyzed the vertical air motion characteristics in the stronger portion

310   of the drafts considered here. However, we found that in many updrafts the strong portion where

311   the vertical velocity is continuously ≥ 1 m s^{-1} dominates and contributes 80% of the total air

312   mass flux, so the statistics of the vertical air motion characteristics in the stronger portion are

313   very similar to those in the draft as a whole. Therefore, the present study focuses on "drafts" in

314   which both weak and strong portions are included.

315

316   **4.   Results**

317   **4.1   Significance of drafts in different strengths**

318   From the analysis above, we note that relatively small and weak updrafts are frequently observed

319   in convective clouds. In this section, we provide further evidence to show the importance of the

320   relatively weak updrafts in terms of air mass flux.

Atmospheric
Chemistry
and Physics
Discussions

321   Fig. 6a shows the average number of updrafts as a function air mass flux observed in the three

322   field campaigns. The solid, dashed and dotted lines represent the penetrations with different

323   diameters. As shown in Fig. 6a, weak and moderate updrafts are more often observed than strong

324   updrafts, and the numbers of updrafts are higher in longer penetrations. Since this is an average

325   result, the number of updrafts could be smaller than 1 (e.g. many narrow penetrations do not

326   have strong updrafts). Fig.6b is similar to Fig. 6a but shows the occurrence frequency of updrafts

327   with different air mass fluxes (i.e. the vertical axis in Fig. 6a is normalized). For the penetrations

328   < 1 km, many of the clouds only have weak or moderate updrafts, and strong updrafts are rarely

329   observed. For penetrations of 1−10 km, the frequency of strong updrafts increases and the

330   frequency of weak and moderate updrafts decreases. For even longer penetrations (>10 km),

331   however, the frequency of weak updrafts increases again, indicating the increasing importance of

332   weak updrafts.

333   Fig. 7 shows the average percentile contributions to the total upward air mass flux by the three

334   different groups of updrafts as a function of penetration diameter. In Fig. 7a, all the penetrations

335   are included. Since many narrow clouds have no strong updrafts in terms of air mass flux, the

336   total air mass flux in these narrow clouds is mostly contributed by weak (red bar) and moderate

337   (green bar) drafts. These narrow clouds may have a high vertical velocity but small air mass flux.

338   As the diameter increases to 4 km, the contributions to total air mass flux from relatively weak

339   updrafts (red bar) decrease, while those from stronger updrafts (blue bar) increase. For a

340   penetration of 4 km, 80%−90% of the total upward mass flux is contributed by the strong

341   updrafts with air mass flux ≥ 500 kg m^{-1} s^{-1}. However, for the penetrations with diameter larger

342   than 4 km, the contribution from relatively weak updrafts increases, probably because more

343   weak updrafts exist in wider clouds (Fig. 6). This is more obvious in Fig. 7b, in which only the

Atmospheric
Chemistry
and Physics
Discussions

Open Access

344   penetrations with at least one strong updraft are included. As the diameter increases from 400 m

345   to 20 km, the contribution from the weak and moderate updrafts (red bars and green bars)

346   increases from 2% to 20%. This suggests that as the cloud evolves and becomes broader (e.g.

347   mature or dissipating stage), the weak and moderate updrafts are also important and therefore

348   necessary to be considered in model simulations.

349

350   **4.2   PDFs of vertical velocity and air mass flux**

351   Fig. 8 shows the PDFs of the vertical velocity in the drafts sampled at 0–2 km, 2–4 km, 4–6 km

352   and higher than 6 km in the three field campaigns. Columns (a), (b) and (c) represent the drafts

353   with air mass flux ≥ 10 kg m^{-1} s^{-1}, ≥ 100 kg m^{-1} s^{-1} and ≥ 500 kg m^{-1} s^{-1} in magnitude,

354   respectively; in other words, column (a) includes all the weak, moderate and strong of drafts,

355   column (b) includes moderate and strong updrafts, and column (c) includes strong updrafts only.

356   For statistical analysis, it is better to analyze different drafts together rather than separately. In all

357   the panels, the vertical velocities are exponentially distributed for both updrafts and downdrafts;

358   the PDFs can be fitted using Eq. (1). From Fig. 8 we can see that at 0–2 km, the PDFs for both

359   COPE and ICE-T are narrow; the updrafts in COPE are slightly stronger than those in ICE-T,

360   while the downdrafts are relatively weaker. At 2–4 km, stronger updrafts and broader PDFs are

361   observed in both COPE and ICE-T compared to those at 0–2 km; the maximum vertical velocity

362   is about 15 m s^{-1}. In COPE, the downdrafts are stronger than those in ICE-T, with the minimum

363   vertical velocity as low as –10 m s^{-1}. For HiCu, the PDFs of the vertical velocity at 2–4 km are

364   narrow, because the HiCu was conducted in the High Plains and the cloud bases are relatively

365   high. At 4–6 km, the updrafts become stronger and the PDFs become broader in all the three

366   field campaigns compared to those at lower levels, especially for COPE and ICE-T. Above 6 km,

367   the PDFs for the updraft become broader in HiCu while they slightly narrow in ICE-T compared

368   to those at 4–6 km. For the downdrafts, the PDFs broaden with height for all the three field

369   campaigns. Generally, the PDFs of the vertical velocity are similar for the three columns. The

370   main difference is found in the first bins of the vertical velocity (0–2 m s^{-1} and – 2–0 m s^{-1}):

371   highest for column (a), which includes all the drafts with air mass flux $\geq$ 10 kg m^{-1} s^{-1} in

372   magnitude, lowest for column (c), which only includes the strong drafts with air mass flux $\geq$ 500

373   kg m^{-1} s^{-1} in magnitude.

374   Generally, the updrafts are stronger in ICE-T or COPE (maritime or coastal convective clouds)

375   than in HiCu (pure continental convective clouds), an observation that differs from earlier studies

376   (e.g. LeMone and Zipser 1980), in which stronger drafts were observed in continental clouds.

377   This is probably because in the previous field campaigns over ocean (e.g. GATE), the aircraft did

378   not penetrate the strongest cores due to safety concerns. Compared to GATE, the PDFs of the

379   vertical velocity in ICE-T has a similar vertical dependence, broadening with height, but the

380   PDFs are broader in ICE-T than those in GATE, and the maximum vertical velocity (25 m s^{-1}) in

381   ICE-T is greater than that observed in GATE (15 m s^{-1}). In addition, convections in continental

382   areas other than the High Plains (e.g. Great Plains) may be different from those in HiCu.

383   Recently, Heymsfield et al. (2010) observed strong updrafts in both maritime and continental

384   convective clouds: most exceed 15 m s^{-1} and some exceed 30 m s^{-1}, but the measurements were

385   made for mature deep convection using airborne Doppler radar. More in-situ measurements are

386   needed to further evaluate the difference between maritime and continental convective clouds,

387   including both developing and mature stages.

Atmospheric
Chemistry
and Physics
Discussions

388   There are a few possible explanations for the stronger updrafts observed in ICE-T and COPE

389   compared to those observed in HiCu. For example, the convective available potential energy

390   (CAPE) is larger in ICE-T than that in HiCu. Typically, the CAPE in ICE-T is greater than 2000

391   J kg^{-1}, and the CAPE in HiCu was less than 100 J kg^{-1}. However, CAPE in COPE is also low

392   (typically less than 100 J kg^{-1}), which cannot explain the relatively strong vertical velocity. The

393   strong vertical velocity in ICE-T and COPE maybe also be related to ice initiation. There are

394   many more millimeter drops in the convective clouds observed in ICE-T (Lawson et al., 2015)

395   and COPE (Leon et al., 2015) than that in HiCu; the millimeter drops can result in fast ice

396   initiation (Lawson et al., 2015), and the significant latent heat released during the ice initiation

397   process can strengthen the vertical velocity. In addition, high concentrations of millimeter drops

398   in ICE-T and COPE can result in the quick formation of graupel and frozen rain drops. The

399   falling graupel and frozen rain drops can strongly enhance the ice generation through ice

400   multiplication processes (Heymsfield and Willis, 2014) and possibly strengthen the updraft.

401   Another difference among the three field campaigns is found in the downdrafts. The downdrafts

402   in HiCu and COPE, which are sampled in mid-latitude convective clouds, are obviously stronger

403   than those in ICE-T, which was conducted over tropical ocean. This may be because the ambient

404   relative humidity is low in HiCu and COPE compared to ICE-T, resulting in a faster evaporation

405   of cloud drops and a stronger cooling effect when ambient air mixes with cloud parcels through

406   lateral entrainment (Heymsfield et al., 1978). But since the diameters of the downdrafts in ICE-T

407   are relatively broader (Fig. 4), the air mass fluxes of the downdrafts are not obviously smaller

408   than that in HiCu and COPE.

409   Fig. 9 shows the PDFs of the air mass flux for all the drafts sampled at 0–2 km, 2–4 km, 4–6 km

410   and higher than 6 km. The PDFs are exponentially distributed for the three field campaigns at

Atmospheric
Chemistry
and Physics
Discussions

411   different heights, which can be fitted using Eq. (1). The coefficients for the fitted function are

412   shown in each panel. At 0–2 km, the PDF of the air mass flux in the updrafts is relatively narrow

413   in ICE-T compared to that in COPE. For the downdraft, the PDF is broader in ICE-T than those

414   in COPE. As height increases up to 6 km, more updrafts with larger air mass flux are observed in

415   ICE-T and the PDFs broadens, but in COPE the PDFs remain similar. In HiCu, the PDFs for

416   updrafts broadens from 2-6 km then remain similar at altitudes higher than 6 km. For downdrafts,

417   the PDFs are similar at different heights for all the three field campaigns. Among the three field

418   campaigns, the differences of the PDFs are small for the weak and moderate drafts and are larger

419   for the strong drafts.

420

421   **4.3   Profiles of vertical velocity and air mass flux**

422   Fig. 10 is a Whisker-Box plot showing the profiles of the vertical velocity (a-c) and air mass flux

423   (d-f) in the drafts based on the three defined thresholds of air mass flux. The solid box includes

424   all the three different groups of drafts, the dashed boxes excludes the weak drafts, and the dotted

425   boxes includes strong drafts only. The minimum, 10%, 50%, 90% and the maximum values are

426   shown in each box. Notice that the vertical velocity and air mass flux in the downdraft is

427   negative, so the minimum value represents the strongest subsiding parcel, the 10% value

428   represents the strongest 10th percentile subsiding parcel, and the 90% value represents the

429   weakest 10th percentile subsiding parcel. This is opposite to the updraft. In each panel, the

430   absolute values of the vertical velocities and air mass flux (except the minimum and maximum

431   ones) are relatively small for the solid boxes.

Atmospheric
Chemistry
and Physics
Discussions

432   In Fig. 10a-c, the three definitions of drafts show different intensities in the vertical velocities.

433   Typically, the 10%, 50% and 90% values in the dotted boxes are 1–2 times larger in magnitude

434   than those in the solid boxes. However, the profiles of the three definitions of drafts vary

435   similarly with height for each field campaign. In the updrafts sampled during HiCu (Fig. 10a),

436   the maximum vertical velocity increases from about 10 m s^{-1} to 18 m s^{-1} with height up to 8 km,

437   then decreases to 14 m s^{-1} at 8–10 km; the 90% vertical velocity in the solid boxes increases from

438   4 m s^{-1} to 8 m s^{-1} between 0–10 km. The 10% and 50% vertical velocities in the solid boxes

439   remain similar between 2–8 km then slightly increase at 8–10 km. The magnitudes of the 10%

440   and 50% vertical velocities in the solid boxes are about 0.5–0.6 m s^{-1} and 1.8–2.5 m s^{-1}. In the

441   downdrafts, the minimum vertical velocity decreases from –7 m s^{-1} to –12 m s^{-1} up to 8 km and

442   increases to –9 m s^{-1} at 8–10 km. The 10%, 50 % and 90% values all slightly decrease with

443   height. In the updrafts sampled during COPE (Fig. 10b), the maximum vertical velocities

444   increase from 8 m s^{-1} to 23 m s^{-1} between 0–6 km, the 10%, 50% and 90% vertical velocities

445   increase up to 6 km. The magnitudes are 0.35–0.45 m s^{-1}, 1–1.6 m s^{-1}, and 2.6–6 m s^{-1} in the solid

446   boxes, respectively. The minimum vertical velocity in the downdrafts intensifies from –5 to –10

447   m s^{-1} with height up to 4 km, then remains similar at 4–6 km. The strongest updraft and

448   downdraft are observed at 4–6 km, about 23 m s^{-1} and -10 m s^{-1}, respectively. In the updrafts

449   sampled during ICE-T (Fig. 10c), the maximum vertical velocities increase with height from 5.5

450   m s^{-1} to 25 m s^{-1} up to 6 km, then slightly decrease at 6–8 km. The 90% value increases from 2 to

451   6 m s^{-1} between 0-4 km, then remains similar at higher levels. The 10% and 50% values, which

452   are about 0.32–0.6 m s^{-1} and 0.8–1.8 m s^{-1} in the solid boxes, respectively, do not show an

453   obvious trend with height. In the downdrafts the minimum vertical velocity increases from –6 m

454   s^{-1} to –5 m s^{-1} between 0 km and 4 km, and decreases from –5 m s^{-1} to –18 m s^{-1} between 4 km

455   and 8 km. The 10%, 50% and 90% values tend to decrease or remain similar at first and then

456   increase with height. The peak (~25 m s^{-1}) and the minimum (~-18 m s^{-1}) vertical velocities are

457   observed at 4–6 km and 6–8 km, respectively.

458   To summarize, vertical velocity in the drafts varies differently with height in the three field

459   campaigns. Generally, the maximum and 90% vertical velocities in the updrafts are greater in

460   COPE or ICE-T than in HiCu, while the median vertical velocities are the greatest in HiCu and

461   weakest in ICE-T. Stronger downdrafts are often observed in HiCu and COPE compared to those

462   in ICE-T. The weak, moderate and strong drafts have similar variations of the vertical velocity

463   with height, but the magnitudes are the smallest when including all the drafts and become larger

464   if the weak drafts are excluded. The 10%, 50% and 90% vertical velocities in updrafts and

465   downdrafts over tropical ocean (ICE-T) observed in this study generally have similar magnitudes

466   to those shown in previous studies (e.g. LeMone and Zipser, 1980; Lucus and Zipser, 1994). But

467   strong updrafts (downdrafts) in excess of 20 m s^{-1} (–10 m s^{-1}) are also observed in this study,

468   which are not shown in pervious aircraft observations. This finding is consistent with recent

469   remote sensing observations (e.g. Heymsfield et al., 2009). The updrafts and downdrafts in

470   convective clouds over land shown in this study (HiCu) are weaker than those shown by Byers

471   and Braham (1949) and Heymsfield et al. (2009), possibly because HiCu was conducted over the

472   High Plains.

473   Fig. 10d-f shows the profiles the air mass flux statistics for the drafts sampled during the three

474   field campaigns. As expected, the absolute values of the air mass flux are relatively small if all

475   the drafts are included (dotted boxes), and become larger if the drafts with small air mass flux are

476   excluded. However, the variations of the air mass flux with height are similar for the three

Atmospheric
Chemistry
and Physics
Discussions

477   different definitions in each panel. As determined by the three thresholds, the minimum absolute

478   values in the solid boxes are about 10 times smaller than those in the dashed boxes and about 50

479   times smaller than those in the dotted boxed; for the 10%, 50%, 90% and the maximum absolute

480   values, the differences among the three type of boxes become smaller. In HiCu, the air mass flux

481   does not show an obvious trend with height. In the updraft, the 10%, 50% and 90% values

482   remain similar at different height ranges. The maximum air mass flux increases from 2–6 km,

483   then decreases with height. The peak value is about 1.3×10^4 kg m^{-1} s^{-1}, found at 4–6 km. The air

484   mass flux in the downdrafts has relatively larger variability, especially for the minimum values.

485   The strongest downdraft in terms of air mass flux (about -1.2×10^4 kg m^{-1} s^{-1}) is found at 4–6 km,

486   but this is probably due to a specific case since the 50% and 90% values are similar to those at

487   the other height ranges. In COPE, the 90% and the maximum air mass flux in the updraft tend to

488   increase with height, while the 10% and 50% values are similar at different height ranges. For

489   the downdraft, the minimum air mass flux decreases between 0–2 km and remains similar at 4-6

490   km. The 10%, 50% and 90% values are similar at different height ranges. The strongest updrafts

491   and downdrafts in terms of air mass flux are observed at 4–6 km and 2–4 km, about 1.8×10^4 kg

492   m^{-1} s^{-1} and -2.8×10^3 kg m^{-1} s^{-1}. In ICE-T, the maximum air mass flux in the updraft increases

493   with height up to 6 km, then decreases at 6–8 km. The 10%, 50% and 90% values in the updraft

494   and downdraft intensify from 0-4 km and decrease or remain similar at higher levels. The

495   strongest updraft (3×10^4 kg m^{-1} s^{-1}) and downdraft (-3.5×10^3 kg m^{-1} s^{-1}) are observed at 4–6 km

496   and 0–2 km, respectively. The minimum value is probably due to a specific case because the

497   10%, 50% and 90% values at 0–2 km are larger or similar to those at the other heights.

498   To summarize, the air mass flux varies with height differently for the three field campaigns. For

499   updraft, the maximum air mass flux is of the order of 10^4 kg m^{-1} s^{-1}, and the median values for

Atmospheric
Chemistry
and Physics
Discussions

500 the three different types of boxes are typically ~100 kg m^{-1} s^{-1}, ~200 kg m^{-1} s^{-1} and ~1000 kg m^{-1}

501 s^{-1}, respectively. The air mass flux in the downdrafts is a few times smaller in magnitude than

502 those in the updrafts, but extreme strong downdraft on the order of 10^4 kg m^{-1} s^{-1} may be

503 observed in some specific cases. Compared to previous studies, the air mass flux in this study

504 shows similar magnitudes, but the vertical dependences are different. Lucas and Zipser (1994)

505 show that the convection off tropical Australia intensifies with height from 0 to 3 km, then

506 weakens with height in terms of air mass flux. Anderson et al. (2005) shows that updrafts and

507 downdrafts over the tropical Pacific Ocean intensify with height up to 4 km, then weaken at

508 higher levels in terms of air mass flux. In the present study, the strongest updrafts and

509 downdrafts are observed at higher levels for all the three field campaigns.

510

511 **4.4   Composite structure of vertical velocity**

512 Fig. 11 shows the composite structure of the vertical velocity as a function of the normalized

513 diameter for the updrafts and downdrafts with air mass flux ≥ 10 kg m^{-1} s^{-1}, 100 kg m^{-1} s^{-1} and

514 500 kg m^{-1} s^{-1} in magnitude. As expected, the draft as a whole is weaker if all the drafts are

515 included in the calculation and becomes stronger if the drafts with small air mass flux are

516 excluded. In HiCu, when all weak, moderate and strong updrafts are included (red curves), the

517 vertical velocity near the center is about 1.7 m s^{-1}. When only moderate and strong updrafts are

518 included (green curves), the vertical velocity near the center is ~2.4 m s^{-1}. When all the updrafts

519 with air mass flux smaller than 500 kg m^{-1} s^{-1} in magnitude are excluded, the absolute values of

520 the vertical velocity near the center increase to ~3.4 m s^{-1}. The vertical velocity in downdrafts is

521 about 0.2 m s^{-1} smaller in magnitude than that in updrafts. The structures of the vertical velocity

Atmospheric
Chemistry
and Physics
Discussions

Open Access

522   in COPE are quite similar to those in HiCu, in both shape and magnitude, especially for the red

523   and green curves. The blue curves have relatively larger variations due to the small sample size.

524   These variations reveal the complicated structure in some drafts. In ICE-T, the shapes of the

525   vertical velocity structures are similar to those in HiCu and COPE, but the magnitudes are

526   smaller, which suggests that statistically more weak drafts are found in ICE-T, although the peak

527   vertical velocity is observed in ICE-T. This is consistent with Fig. 10. In Fig. 11, if the

528   magnitude of the vertical velocity is normalized, the structures of the three defined classes of

529   updraft and downdraft among the three field campaigns will be very similar.

530   In this composite analysis based on in-situ measurements, the penetration direction has no

531   obvious impact on the vertical velocity structure, whether the aircraft penetrates along or across

532   the horizontal wind. For convective cloud, wind shear has a large impact on the cloud evolution

533   (Weisman and Klemp 1982); however, aircraft data are insufficient to reveal the wind shear

534   impact, because each penetration is made at a single level and the aircraft does not always

535   penetrate through the center of the draft. Remote sensing data can be helpful to study the two-

536   dimensional or three-dimensional structures of the vertical velocity in convective clouds (e.g.

537   Wang and Geerts, 2013). Thus, in-situ measurements as well as remote sensing measurements

538   are needed to further analyze the wind shear impact.

539

540   **4.5   Vertical air motion characteristics as clouds evolve**

541   Fig. 12 shows the profiles of the vertical velocity (a-c) and the air mass flux (d-f) for the updraft

542   and downdraft in the convective clouds with different cloud top heights (CTH). Here, all weak,

Atmospheric
Chemistry
and Physics
Discussions

543   moderate and strong updrafts are included. Different colors represent the clouds with different

544   CTHs. These profiles can generally reveal the change of vertical velocity and air mass flux as the

545   clouds evolve. The key point presented in Fig. 12 is that the peak vertical velocity and air mass

546   flux is observed at higher levels as the clouds evolve. For clouds with CTHs lower than 4 km

547   (red boxes), the maximum vertical velocity is observed at 2–4 km. When the cloud become

548   deeper, the vertical velocity and air mass flux are stronger at higher levels. This is to be expected,

549   because all the data analyzed in this paper are collected from isolated convective clouds, so the

550   convective bubbles keep ascending as the clouds evolve. MCSs may have different

551   characteristics of vertical air motion because there is continuous low level convective source.

552   The maximum vertical velocity is observed within 2 km below cloud top; this is consistent with

553   Doppler velocity images measured by WCR (e.g. Fig. 2b), which show the typical strongest

554   updraft is observed 1–1.5 km below cloud top. The strongest downdrafts are sometimes observed

555   more than 2 km below cloud top. The 10%, 50% and 90% values do not have obvious trend as

556   the clouds evolve, especially in HiCu and ICE-T, possibly because of the increasing contribution

557   from moderate and weak drafts as the clouds become deeper and broader (Fig. 6 and 7).

558   Generally, in HiCu and ICE-T the drafts intensify as the clouds evolve, but this is not found in

559   COPE, maybe because most of the penetrations were made near the cloud top, rather than in the

560   strongest portion of a draft. Since the vertical resolution of aircraft in-situ data is poor, more data,

561   including remote sensing measurements, are needed to better understand the evolution of the

562   vertical velocity in convective clouds as they go through the different stages..

563

564   **5.   Conclusions**

Atmospheric
Chemistry
and Physics
Discussions

565   The vertical velocity and air mass flux in convective clouds are statistically analyzed in this

566   study using aircraft data collected from three field campaigns, HiCu, COPE and ICE-T,

567   conducted over mid-latitude High Plains, mid-latitude coastal area and tropical ocean. Three

568   thresholds of air mass flux are selected to delineate draft: 10 kg m^{-1} s^{-1}, 100 kg m^{-1} s^{-1} and 500 kg

569   m^{-1} s^{-1} in magnitude. The main findings are as follows.

570   1)   Small-scale updrafts and downdrafts in convective clouds are often observed in the three

571   field campaigns. More than 85%, 90% and 74% of the updrafts are narrower than 500 m in HiCu,

572   COPE and ICE-T, respectively, and more than 90 % of the downdrafts are narrower than 500 m

573   in the three field campaigns combined. These small scale drafts make significant contributions to

574   the total air mass flux. Updrafts narrower than 500 m contribute 20%−35% of the total upward

575   flux, and downdrafts narrower than 500 m contribute 50%−65% of the total downward air mass

576   flux.

577   2)   In terms of the air mass flux, the weak and moderate drafts make an important

578   contribution to the total air mas flux exchange. Generally, the number of drafts increases with

579   cloud diameter. For many narrow clouds, the weak and moderate drafts dominate and contribute

580   most of the total air mass flux. For broader clouds, the stronger updrafts contribute most of the

581   total air mass flux, but the contribution from weak and moderate drafts increases as the cloud

582   evolves.

583   3)   PDFs and profiles of the vertical velocity are provided for the three defined types of

584   drafts. In all the height ranges, the PDFs are roughly exponentially distributed. At the lowest

585   level, the PDFs of the vertical velocity are relatively narrow, and broaden with height. For the

586   updrafts, the PDFs of the vertical velocity are broader in ICE-T and COPE, while for the

Atmospheric
Chemistry
and Physics
Discussions

587   downdrafts the PDFs of the vertical velocity are broader in HiCu and COPE. The profiles show

588   that updrafts are stronger in ICE-T and COPE than in HiCu, and downdrafts are stronger in HiCu

589   and COPE compared to ICE-T.

590   4)   PDFs and profiles of the air mass flux are provided for the drafts. The PDFs are similarly

591   exponentially distributed at different heights. For updrafts, the PDFs are broader in ICE-T than in

592   HiCu and COPE, but for downdrafts the PDFs are broader in HiCu and COPE than in ICE-T. In

593   the updrafts, the maximum air mass flux has an order of 10^4 kg m^{-1} s^{-1}. The air mass flux in the

594   downdrafts are typically a few times smaller in magnitude than those in the updrafts.

595   5)   The composite structures of the vertical velocity in the updrafts and downdrafts have

596   similar shapes for the three field campaigns: the vertical velocity is the strongest near the center,

597   and weakens towards the edges. On average, the updrafts have similar intensity across the three

598   field campaigns, while for downdrafts the vertical velocity is the weakest in ICE-T and stronger

599   in HiCu and COPE.

600   6)   The change of vertical air motion characteristics as the cloud evolves are briefly

601   discussed. Generally, the strongest portion of a draft ascends with height as the cloud evolves.

602   The maximum vertical velocity is observed within 2 km below cloud top; the downdrafts are

603   sometimes stronger at levels more than 2 km below cloud top.

604   Based on the aircraft observations from three field campaigns, this study provides quantitative

605   analyses of the vertical air motion characteristics in isolated convective clouds, compares the

606   differences of vertical velocity and air mass flux among the different field campaigns, and shows

607   the importance of small-scale updrafts and downdrafts. The results are useful to evaluate model

Atmospheric
Chemistry
and Physics
Discussions

Open Access

EGU

608   simulations and improve parameterizations in models. To better understand the differences of the

609   vertical air motions among different convective clouds and the evolution of the updrafts and

610   downdrafts in convective clouds more data are needed.

611

612   **Acknowledgments**

618

Atmospheric
Chemistry
and Physics
Discussions

Open Access

References

619 **References**

620 Anderson, N. F., Grainger, C. A., and Stith, J. L.: Characteristics of Strong Updrafts in

621 Precipitation Systems over the Central Tropical Pacific Ocean and in the Amazon. J. Appl.

622 Meteor., 44, 731–738, 2005.

623 Arakawa, A.: The cumulus parameterization problem: Past, present, and future. J. Clim., 17,

624 2493–2525, 2004.

625 Bechtold, P., Bazile, E., Guichard, F., Mascart, P. and Richard, E.: A mass-flux convection

626 scheme for regional and global models. Quarterly Journal of the Royal Meteorological

627 Society, 127(573), 869-886, 2001.

628 Byers, H. R. and Braham, R. R.: The Thunderstorm-Report of the Thunderstorm Project. U.S.

629 Weather Bureau, Washington, D.C., Jun 1949. 287 pp. [NTIS PB234515], 1949.

630 Del Genio, A. D., Wolf, A. B., and Yao, M.-S.: Evaluation of regional cloud feedbacks using

631 single-column models, J. Geophys. Res., 110, D15S13, doi:10.1029/2004JD005011, 2005.

632 Donner, L. J., Seman, C. J., Hemler, R. S., and Fan, S.: A Cumulus Parameterization Including

633 Mass Fluxes, Convective Vertical Velocities, and Mesoscale Effects: Thermodynamic and

634 Hydrological Aspects in a General Circulation Model. J. Climate, 14, 3444–3463, 2001.

635 Heymsfield, A. J., Johnson, P. N., and Dye, J. E.: Observations of Moist Adiabatic Ascent in

636 Northeast Colorado Cumulus Congestus Clouds. J. Atmos. Sci., 35, 1689–1703, 1978.

637   Heymsfield, A. J., and Willis, P.: Cloud conditions favoring secondary ice particle production in

638   tropical maritime convection. J. Atmos. Sci., 71, 4500–4526, 2014.

639   Heymsfield, G. M., Tian, L., Heymsfield, A. J., Li, L., and Guimond, S.: Characteristics of Deep

640   Tropical and Subtropical Convection from Nadir-Viewing High-Altitude Airborne Doppler

641   Radar. J. Atmos. Sci., 67, 285–308, 2010.

642   Hogan, R. J., Grant, A. L., Illingworth, A. J., Pearson, G. N., and O'Connor, E. J.: Vertical

643   velocity variance and skewness in clear and cloud-topped boundary layers as revealed by

644   Doppler lidar, Q. J. Roy. Meteorol. Soc., 135, 635–643, 2009.

645   Houze Jr., R. A., and Betts, A. K.: Convection in GATE, Rev. Geophys., 19(4), 541–576, 1981.

646   Igau, R. C., LeMone, M. A., and Wei, D.: Updraft and Downdraft Cores in TOGA COARE:

647   Why So Many Buoyant Downdraft Cores?. J. Atmos. Sci., 56, 2232–2245, 1999.

648   Ivanova, I. T. and Leighton, H. G.: Aerosol–Cloud Interactions in a Mesoscale Model. Part I:

649   Sensitivity to Activation and Collision–Coalescence. J. Atmos. Sci., 65, 289–308, 2008.

650   Jorgensen, D. P., Zipser, E. J., and LeMone, M. A.: Vertical Motions in Intense Hurricanes. J.

651   Atmos. Sci., 42, 839–856, 1985.

652   Jorgensen, D. P. and LeMone, M. A.: Vertically Velocity Characteristics of Oceanic Convection.

653   J. Atmos. Sci., 46, 621–640, 1989.

654   Khairoutdinov, M. F., Krueger, S. K., Moeng, C.-H., Bogenschutz, P. A., and Randall, D. A.:

655   Large-Eddy Simulation of Maritime Deep Tropical Convection, J. Adv. Model. Earth Syst., 1, 15,

656   doi:10.3894/JAMES.2009.1.15, 2009.

657   Khelif, D., Burns, S. P., and Friehe, C. A.: Improved Wind Measurements on Research

658   Aircraft. J. Atmos. Oceanic Technol., 16, 860–875, 1999.

659   Kollias, P and Albrecht, B.: Vertical Velocity Statistics in Fair-Weather Cumuli at the ARM

660   TWP Nauru Climate Research Facility. J. Climate, 23, 6590–6604, 2010.

661   Lawson, P. R., Woods, S., and Morrison, H.: The microphysics of ice and precipitation

662   development in tropical cumulus clouds. J. Atmos. Sci., 72, 2429-2445, 2015.

663   LeMone, M. A., and Zipser, E. J.: Cumulonimbus vertical velocity events in GATE. Part I:

664   Diameter, intensity and mass flux. J. Atmos. Sci., 37, 2444–2457, 1980.

665   Leon, D., and co-authors: The COnvective Precipitation Experiment (COPE): Investigating the

666   origins of heavy precipitation in the southwestern UK. Bull. Amer. Meteor. Soc.

667   doi:10.1175/BAMS-D-14-00157.1, in press, 2015.

668   Lucas, C., Zipser, E. J., and Lemone, M. A.: Vertical Velocity in Oceanic Convection off

669   Tropical Australia. J. Atmos. Sci., 51, 3183–3193, 1994.

670   May, P. T. and Rajopadhyaya, D. K.: Vertical Velocity Characteristics of Deep Convection over

671   Darwin, Australia. Mon. Wea. Rev., 127, 1056–1071, 1999.

672   Schmeter, S. M.: Structure of fields of meteorological elements in a cumulonimbus zone, Hydro.

673   Meteor. Serv., Trans. Cent. Aerol. Obs. [Trans. From Russian by Israel Prog. For Sci. Trans.,

674   Jerusalem, 1970, 117 pp.], 1969.

675   Schumacher, C., Stevenson, S. N., and Williams, C. R.: Vertical motions of the tropical

676   convective cloud spectrum over Darwin, Australia. Q.J.R. Meteorol. Soc.. doi: 10.1002/qj.2520,

677   2015.

678   Tiedtke, M.: A comprehensive mass flux scheme for cumulus parameterization in large-scale

679   models. Monthly Weather Review, 117(8), 1779-1800, 1989.

680   Tonttila, J., O'Connor, E. J., Niemelä, S., Räisänen, P., and Järvinen, H.: Cloud base vertical

681   velocity statistics: a comparison between an atmospheric mesoscale model and remote sensing

682   observations. Atmos. Chem. Phys., 11, 9207-9218, 2011.

683   Wang, X., and Zhang M.: Vertical velocity in shallow convection for different plume types, J.

684   Adv. Model. Earth Syst., 6, 478–489, 2014.

685   Wang, Y. and Geerts, B.: Composite Vertical Structure of Vertical Velocity in Nonprecipitating

686   Cumulus Clouds. Mon. Wea. Rev., 141, 1673–1692, 2013.

687   Wang, Z. and co-authors: Single aircraft integration of remote sensing and in situ sampling for

688   the study of cloud microphysics and dynamics. Bull. Amer. Meteor. Soc., 93, 653–668, 2012.

689   Weisman, M. L. and Klemp, J. B.: The dependence of numerically simulated convective storms

690   on vertical wind shear and buoyancy. Monthly Weather Review, 110, 504-520, 1982.

691   Wendisch, M., and Brenguier, J.: Airborne Measurements for Environmental Research: Methods

692   and Instruments. Wiley, 520 pages, 2013.

693   Wu, J., Del Genio, A. D., Yao, M.-S., and Wolf, A. B.: WRF and GISS SCM simulations of

694   convective updraft properties during TWP-ICE, J. Geophys. Res., 114, D04206,

695   doi:10.1029/2008JD010851, 2009.

696   Zipser, E. J., Cecil, D. J., Liu, C., Nesbitt, S. W., and Yorty, D. P.: Where are the most intense

697   thunderstorms on Earth?. Bull. Amer. Meteor. Soc., 87, 1057–1071, 2006.

698

Table 1. Number of penetrations, time in clouds and flight length in clouds sampled at 0–2 km, 2–4 km, 4–6 km, 6–8 km and 8–10 km MSL in HiCu, COPE and ICE-T.

Height (km MSL)	HiCu			COPE			ICE-T		
	Number of penetrations	Time in clouds (min)	Length in clouds (km)	Number of penetrations	Time in clouds (min)	Length in clouds (km)	Number of penetrations	Time in clouds (min)	Length in clouds (km)
8–10	43	12	79						
6–8	565	122	789				132	52	423
4–6	596	104	653	207	39	244	299	116	895
2–4	373	50	274	378	86	486	34	10	73
0–2				219	40	211	197	27	167

35

Atmospheric
Chemistry
and Physics
Discussions

Table 2. Number of updrafts and downdrafts sampled at 0-2 km, 2-4 km, 4-6 km, 6-8 km and 8-10 km in HiCu, COPE and ICE-T.

Three numbers are given for the updraft and downdraft at each level, respectively, according to the three different definitions: weak, moderate and strong.

Height (km)		HiCu		COPE		ICE-T	
		Updraft	Downdraft	Updraft	Downdraft	Updraft	Downdraft
8-10	weak	66	100				
	moderate	52	44				
	strong	44	17				
6-8	weak	818	763			382	372
	moderate	559	540			175	136
	strong	287	130			102	23
4-6	weak	748	668	290	184	858	671
	moderate	522	389	232	193	425	329
	strong	343	48	135	51	266	73
2-4	weak	311	235	568	424	49	47
	moderate	271	84	467	434	51	51
	strong	149	7	188	101	32	10
0-2	weak			368	192	319	205
	moderate			266	90	234	104
	strong			96	9	60	7

Atmospheric
Chemistry
and Physics
Discussions
Open Access
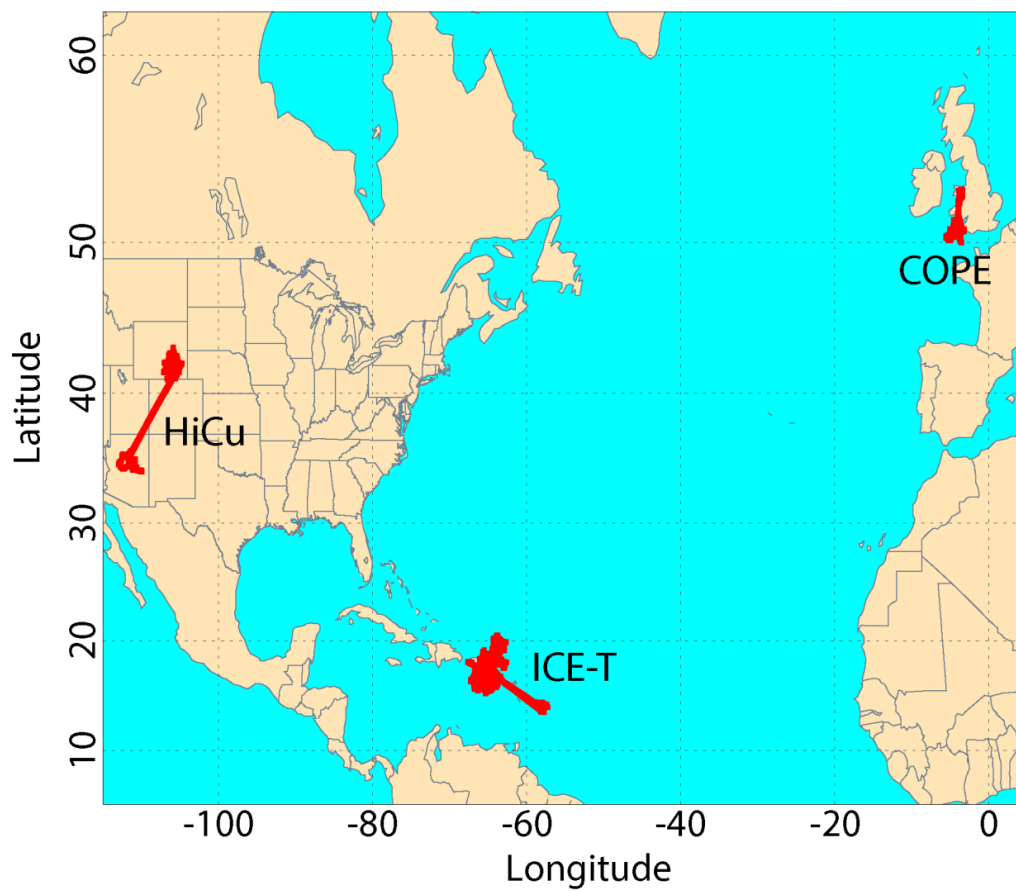
Figure 1. Flight tracks for the three field campaigns: HiCu, COPE and ICE-T.
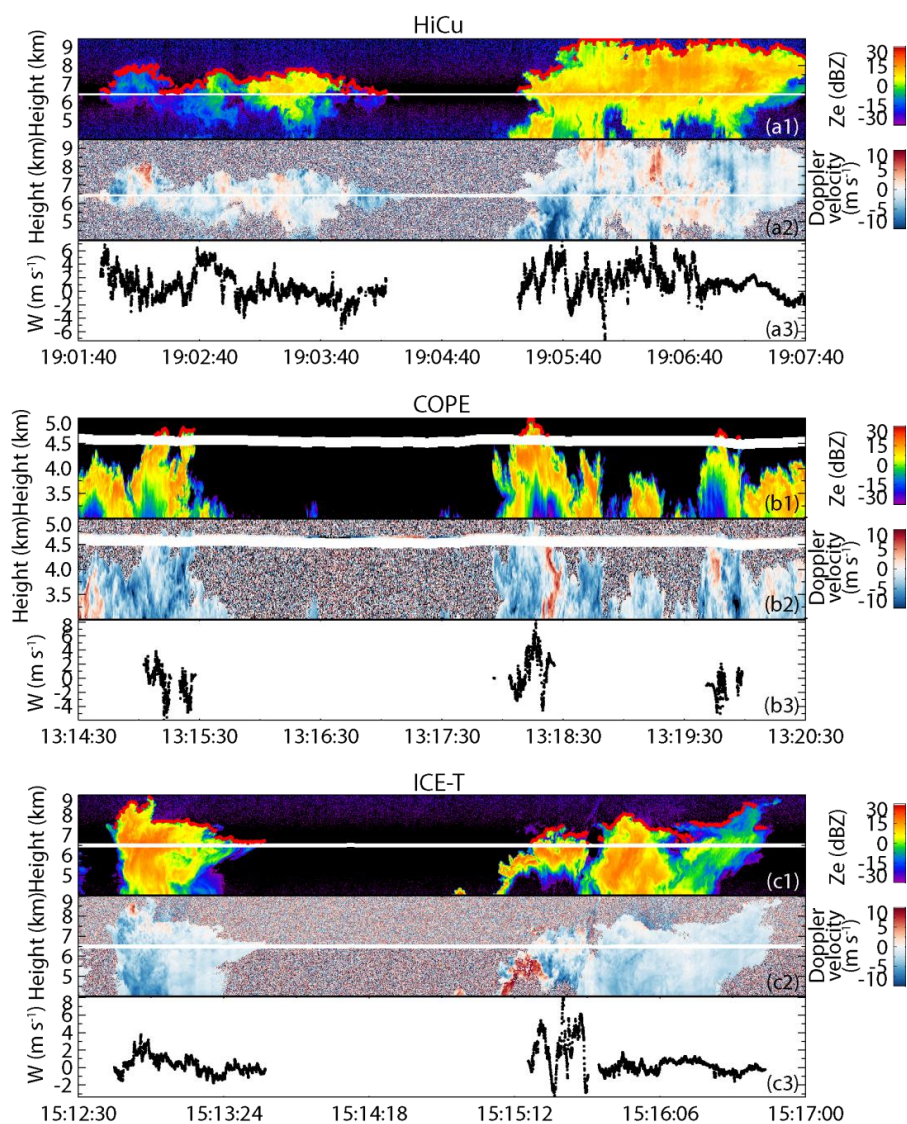
Figure 2. Examples of radar reflectivity, Doppler velocity and 25-Hz in-situ vertical velocity measurements for the convective clouds sampled in HiCu, COPE and ICE-T. The red dots in (a1), (b1) and (c1) are the cloud tops estimated by WCR.
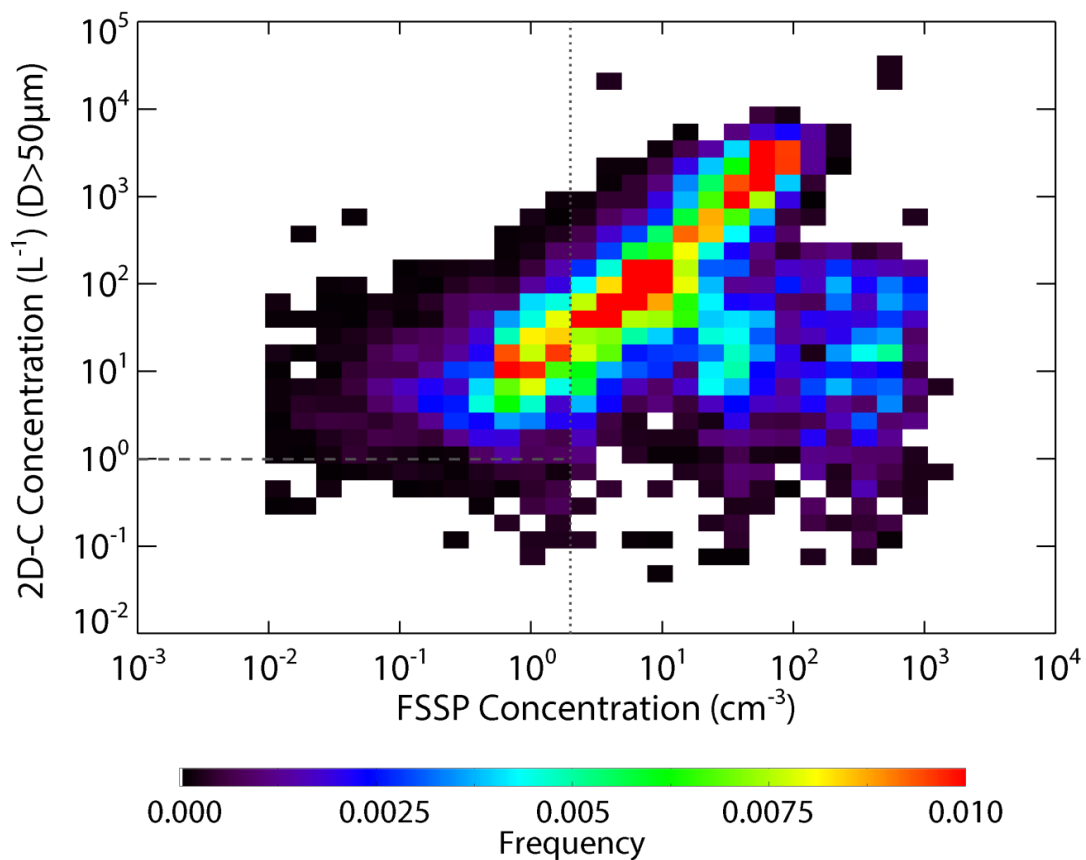
Figure 3. Occurrence distributions as a function of the particle concentrations measured by FSSP versus the concentrations of the particles ≥ 50 μm in diameter measured by 2D-C in the clouds identified by WCR reflectivity. The dashed and dotted lines indicate the FSSP concentration equal 2 cm^{-3} and the 2D-C concentration equal 1 L^{-1}, respectively.
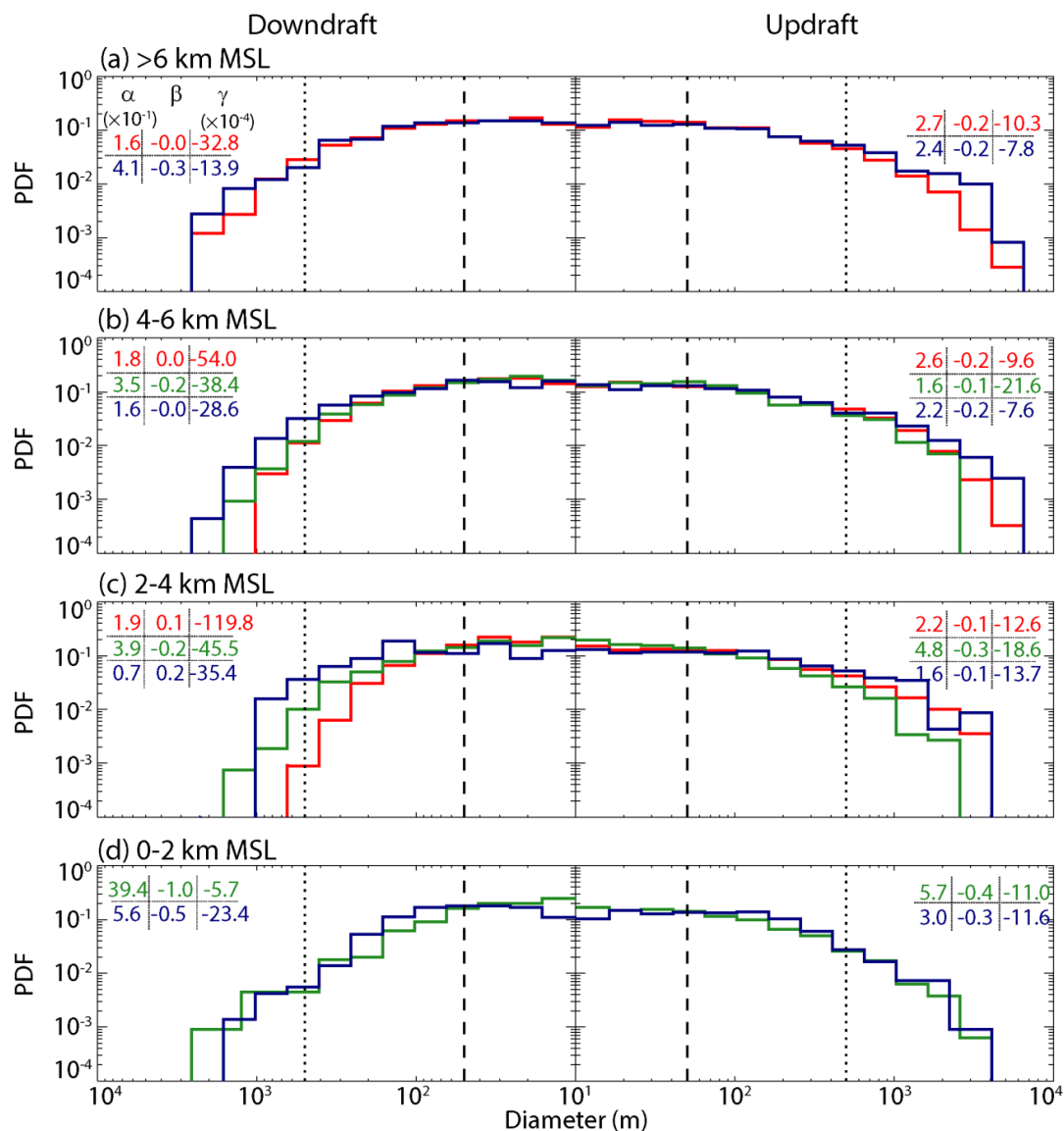
Figure 4. PDFs of the diameters for the updrafts and downdrafts sampled at 0–2 km, 2–4 km, 4–6 km and higher than 6 km. The numbers shown in each panel are the coefficients of the fitted exponential function (Eq. 1).
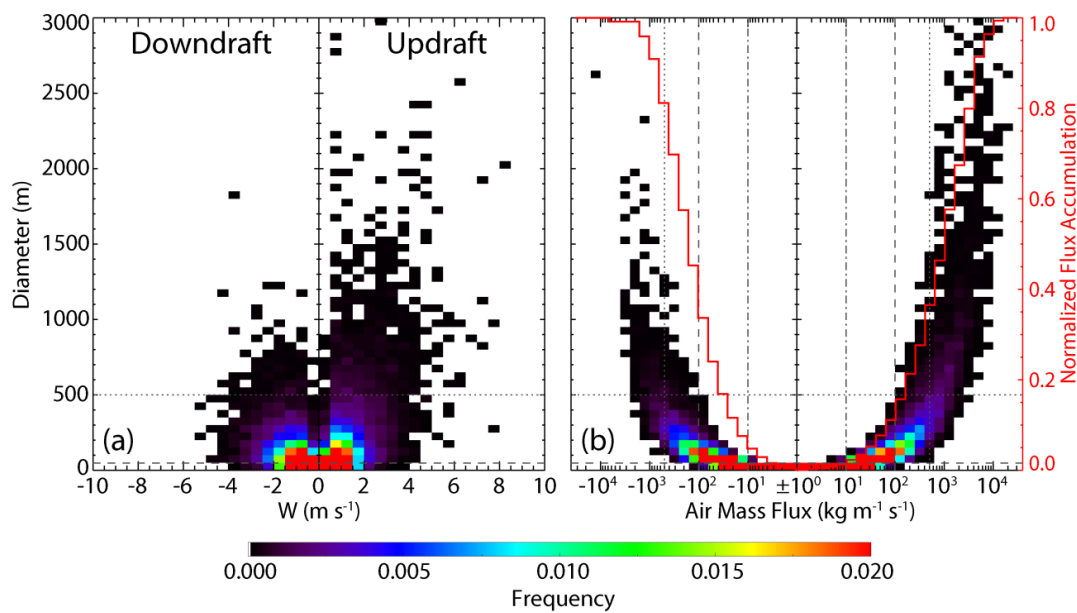
Figure 5. Occurrence distributions as (a) a function of diameter and mean vertical velocity, and (b) a function of diameter and air mass flux for all updrafts and downdrafts. The normalized accumulation flux is also shown by the red curves. The horizontal dotted and dashed lines in (a) and (b) indicate the draft diameter equal 500 m and 50 m, which are used as the diameter thresholds to identify a "draft" in previous studies and in this study, respectively. The vertical dash-dotted, dashed and dotted lines in (b) indicate air mass flux equal 10 kg m^{-1} s^{-1}, 100 kg m^{-1} s^{-1} and 500 kg m^{-1} s^{-1} in magnitude, respectively, which are the thresholds used to delineate the three different groups of draft.

Atmospheric
Chemistry
and Physics
Discussions

Open Access

EGU
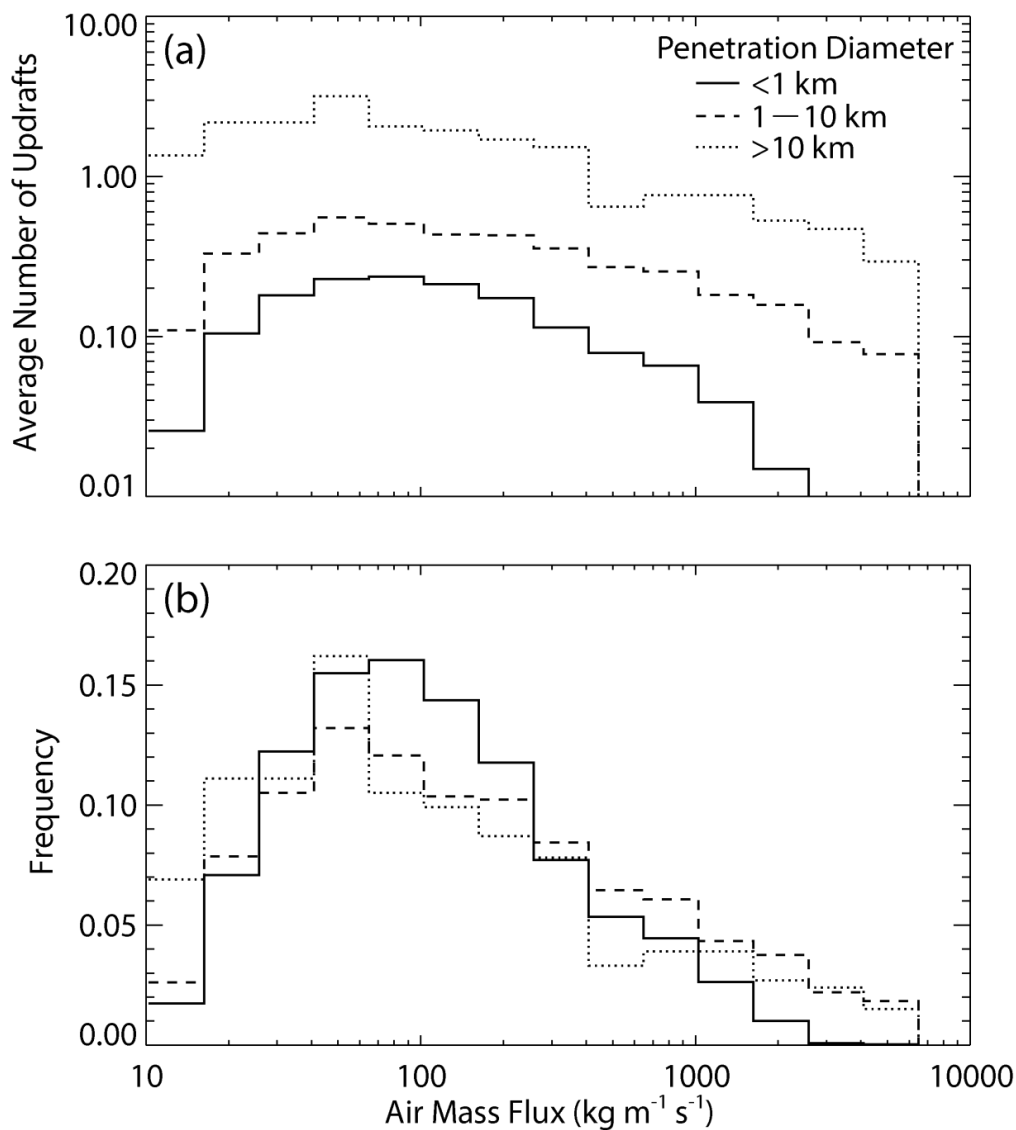
Figure 6. (a) Average number and (b) occurrence frequency of updrafts as a function of air mass flux observed in penetrations with length < 1 km (solid), 1-10 km (dashed) and >10 km (dotted). The result is a composite of HiCu, COPE and ICE-T.

Atmospheric
Chemistry
and Physics
Discussions

Open Access

EGU
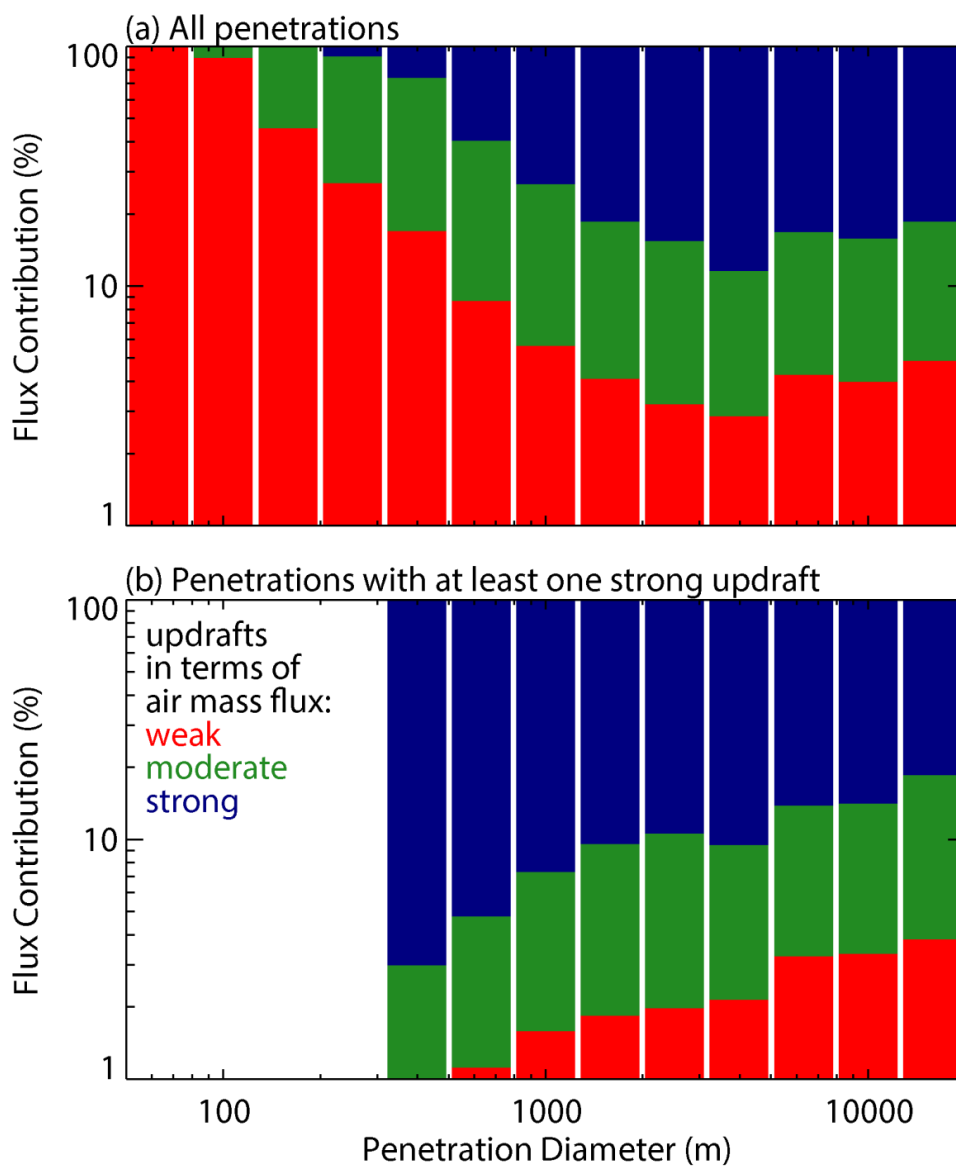
Figure 7. Average percentile contribution to total upward air mass flux by the weak (red),

moderate (green) and strong (blue) updrafts delineated in this study. The result is a composite of

HiCu, COPE and ICE-T.
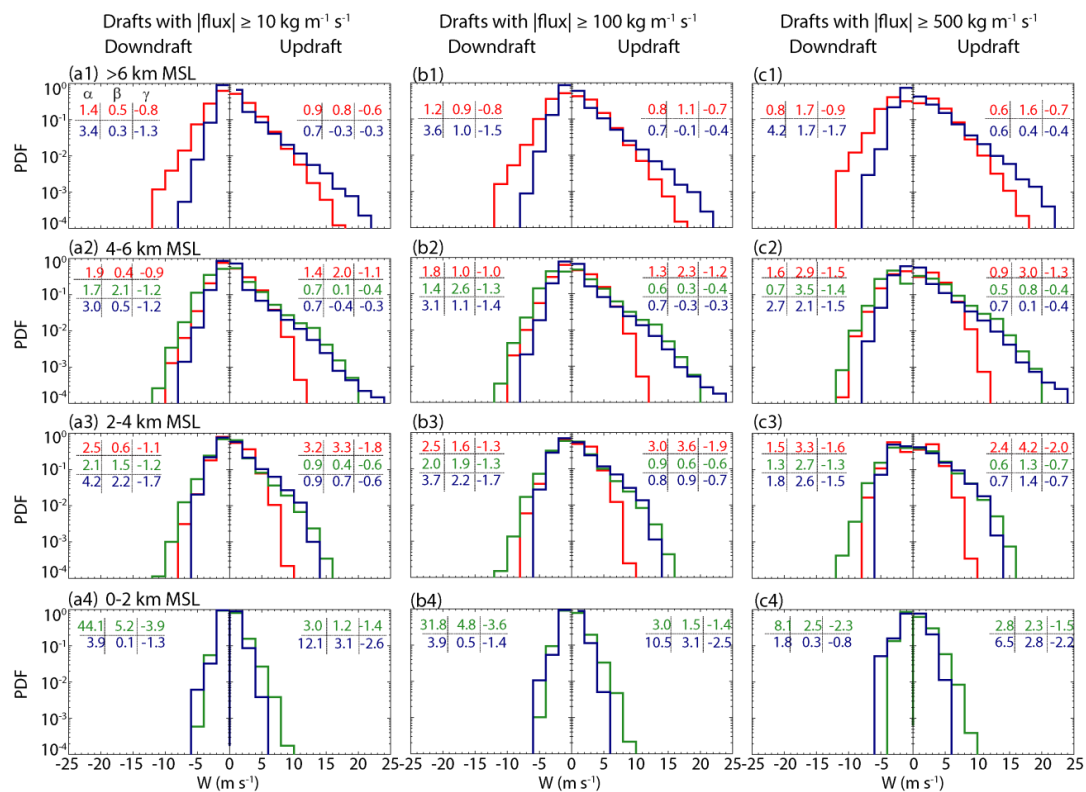
Figure 8. PDFs of the 25-Hz vertical velocity for the updrafts and downdrafts with air mass flux $\geq$ (a) 10 kg m^{-1} s^{-1}, (b) 100 kg m^{-1} s^{-1} and (c) 500 kg m^{-1} s^{-1} in magnitude, sampled at 0–2 km, 2–4 km, 4–6 km and higher than 6 km. The numbers shown in each panel are the coefficients of the fitted exponential function (Eq. 1).
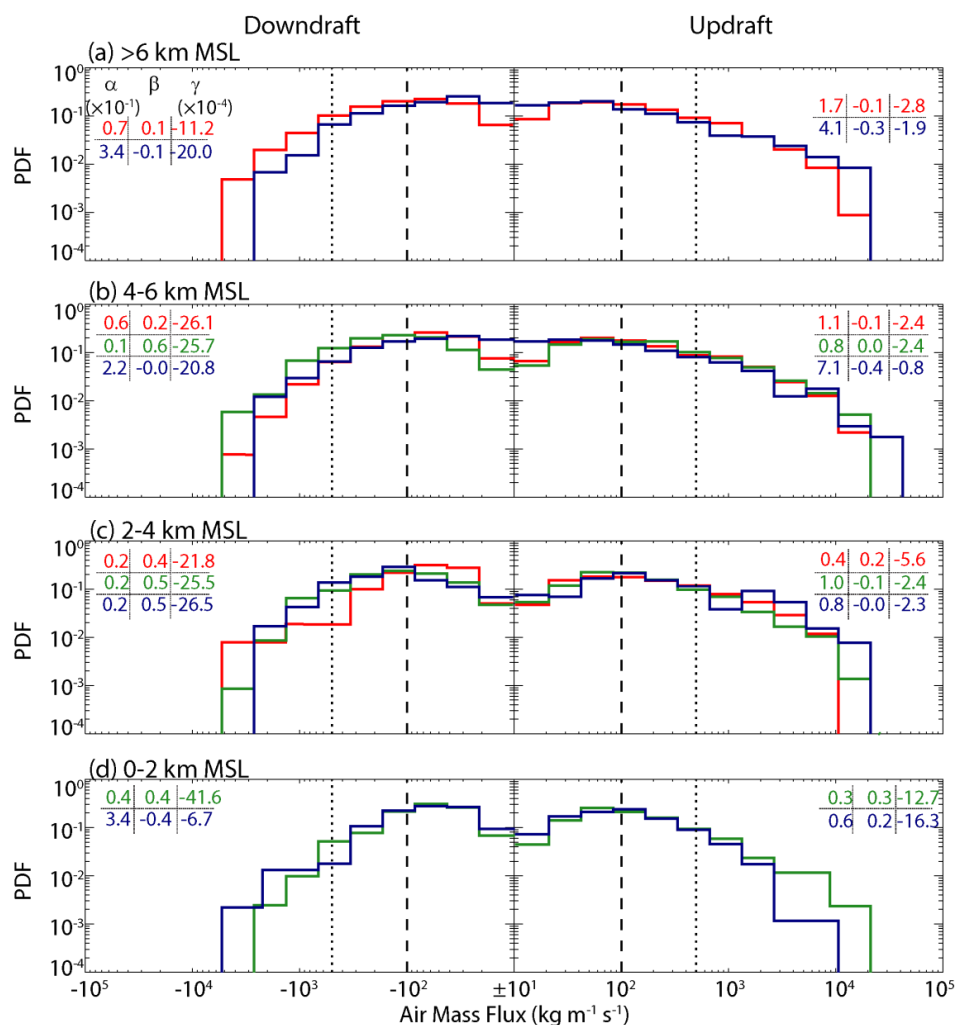
Figure 9. PDFs of the air mass flux for the updrafts and downdrafts sampled at 0–2 km, 2–4 km, 4–6 km and higher than 6 km. The three thresholds of the air mass flux (± 10 kg m^{-1} s^{-1}, ± 100 kg m^{-1} s^{-1} and ± 500 kg m^{-1} s^{-1}) are shown by the solid (overlaps with the central y-axis in each panel), dashed and dotted lines. The numbers shown in each panel are the coefficients of the fitted exponential function (Eq. 1).

Atmospheric
Chemistry
and Physics
Discussions

Open Access
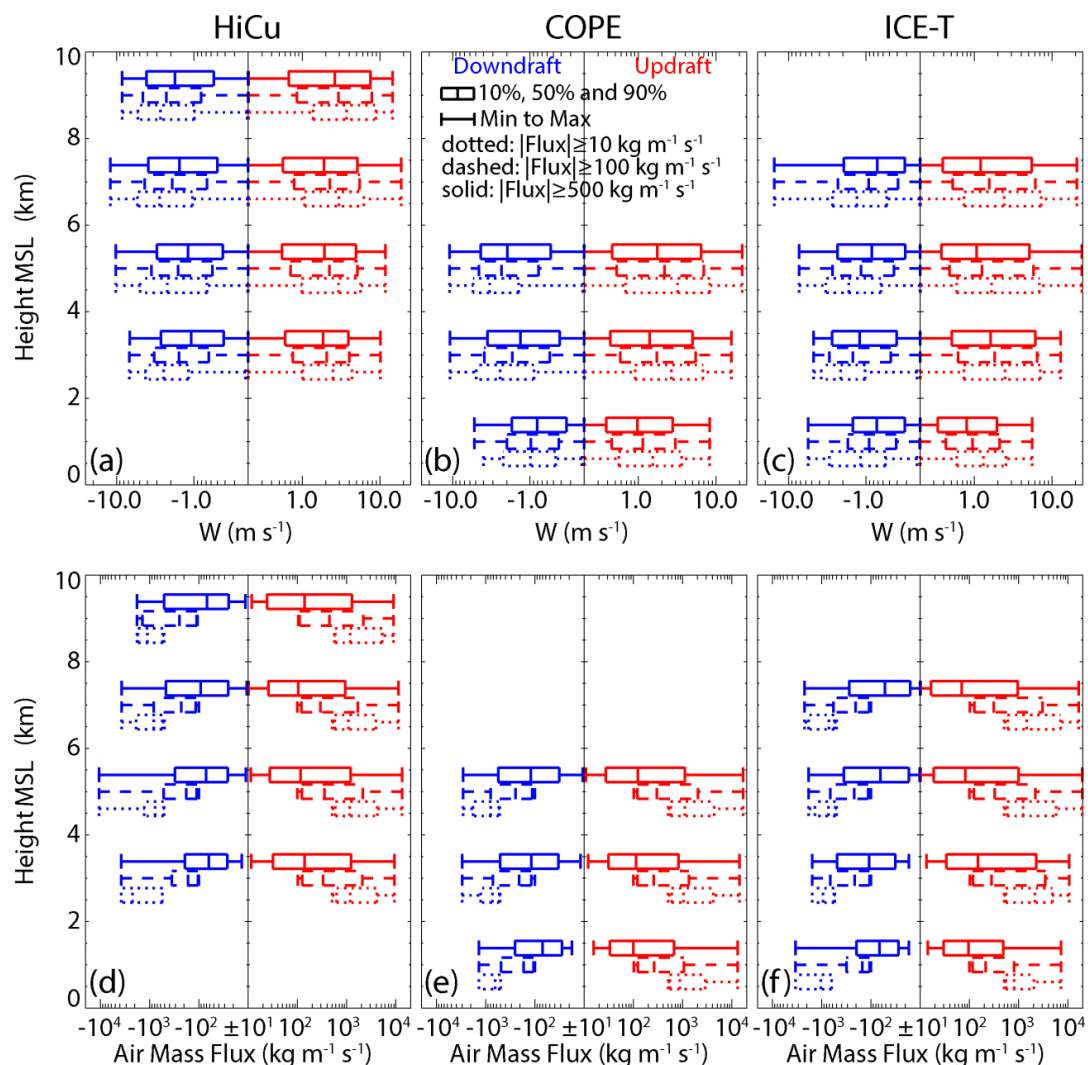
Figure 10. Profiles of (a-c) the vertical velocity and (d-f) air mass flux for all the updrafts and downdrafts sampled at 0–2 km, 2–4 km, 4–6 km, 6–8 km and 8–10 km. The dotted, dashed and solid boxes represent for the drafts with air mass flux ≥ 10 kg m^{-1} s^{-1}, 100 kg m^{-1} s^{-1} and 500 kg m^{-1} s^{-1} in magnitude, respectively.
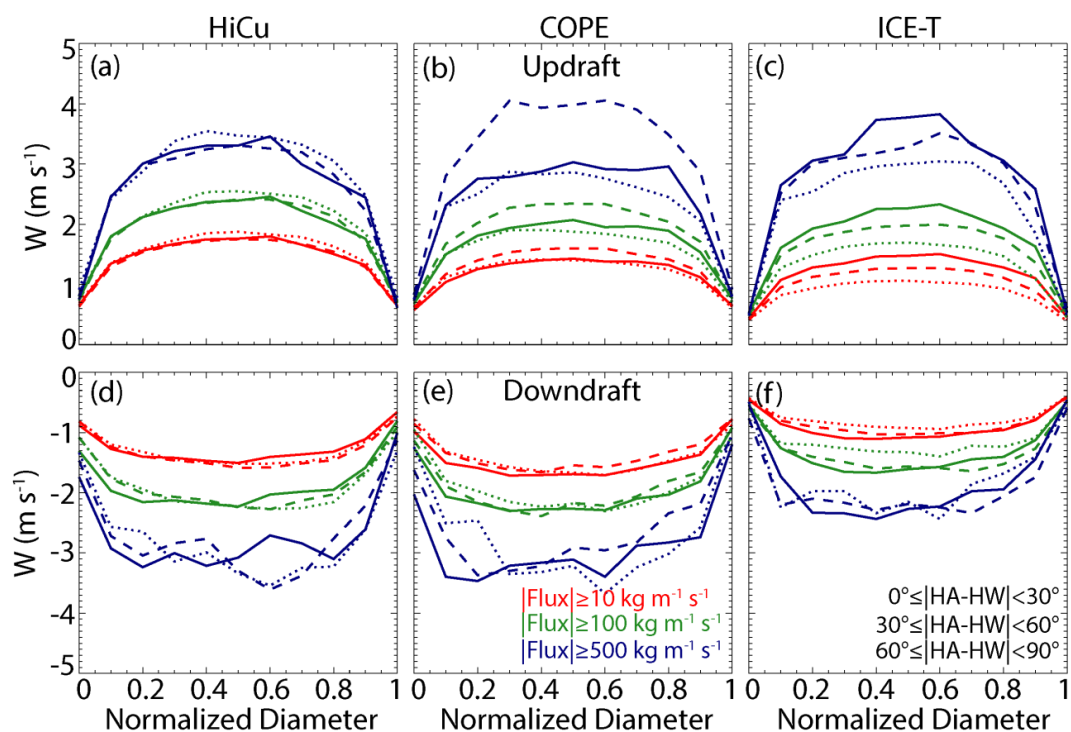
Figure 11. Composite structure of the vertical velocity as a function of the normalized diameter for the updrafts and downdrafts with air mass flux ≥ 10 kg m^{-1} s^{-1}, 100 kg m^{-1} s^{-1} and 500 kg m^{-1} s^{-1} in magnitude. The solid, dashed and dotted curves represent penetrations with the heading angles (HA) 0°–30°, 30°–60° and 60°–90° from the horizontal wind (HW) directions, respectively. The 0 and 1 coordinates on the x-axis indicate the upwind and downwind sides of the draft.
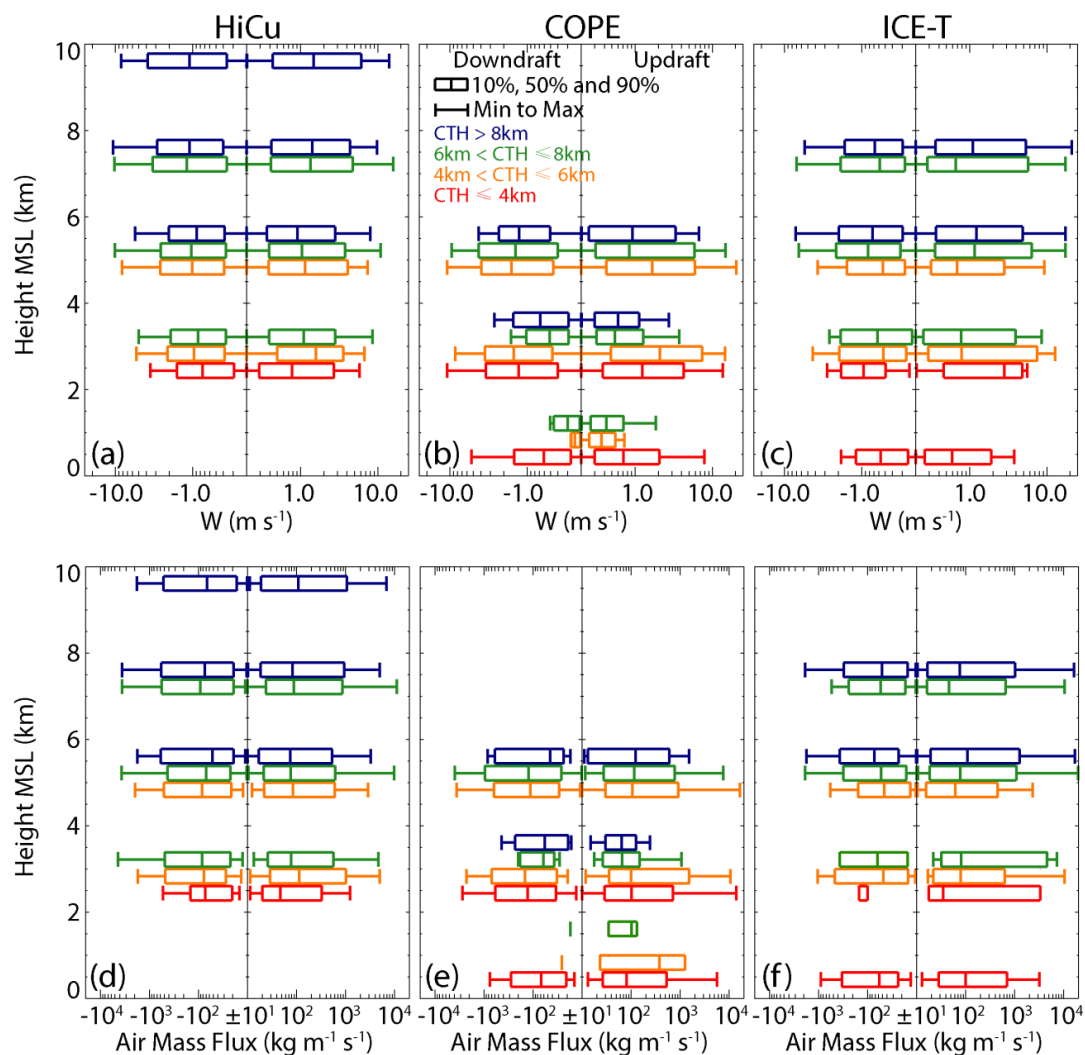
Figure 12. Profiles of (a-c) the vertical velocity and (d-f) the air mass flux for the updraft and downdraft with air mass flux ≥ 10 kg m^{-1} s^{-1} in magnitude. The red, orange, green and blue boxes represent clouds with cloud top heights of 0-4 km, 4-6 km, 6-8 km and higher than 8 km.